Eulerian Scheme for 3D multimaterials

Alexia de Brauer, Angelo Iollo, Thomas Milcent

To cite this version :

Alexia BRAUER (DE), Angelo IOLLO, Thomas MILCENT - Eulerian Scheme for 3D multimaterials - In: Eighth International Conference on Computational Fluid Dynamics (ICCFD8(8; 2014 ; Chine), China, 2014-07 - Eighth International Conference on Computational Fluid Dynamics (ICCFD8) - 2014

Eulerian Scheme for 3D multimaterials

Alexia de Brauer[1], Angelo Iollo[1] & Thomas Milcent [2]

[1]Institut de Mathématiques de Bordeaux, UMR CNRS 5251, Université de Bordeaux et
Inria Bordeaux - Sud Ouest, 33405 Talence, France
[2]Institut de Mécanique et d'Ingénierie, UMR CNRS 5295, Université de Bordeaux et
Arts et Métiers Paritech, 33405 Talence, France

Corresponding author: angelo.iollo@math.u-bordeaux1.fr

Abstract: This paper is devoted to the 3D extension of a sharp interface multimaterial method. We present preliminary results for 3D stiff cases of shock air/helium/water interaction and impacts of projectiles on elastic bodies immersed in air.

Keywords: Compressible multimaterial, Cartesian mesh, Eulerian elasticity, HLLC Riemann Solver.

1   Introduction

Physical and engineering problems that involve several materials are ubiquitous in nature and in applications. The main contributions in the direction of simulating these phenomena go back to [1]. We have already developed a numerical scheme to solve the Eulerian equations for multimaterial (see [2] and [3] for 1D numerical results and [4] for 2D results). This scheme is based on a directional splitting on a fixed Cartesian mesh where the fluxes are computed by a HLLC approximate Riemann solver. This paper is devoted to the extension of this method in 3D, where two additional elastic waves corresponding to a torsion perturbation are present.

2   The Eulerian Model

The conservative form of elastic media equations in the Eulerian framework are

$$\begin{cases} \rho_t + \operatorname{div}_x(\rho u) = 0 \\ (\rho u)_t + \operatorname{div}_x(\rho u \otimes u - \sigma) = 0 \\ (\nabla_x Y)_t + \nabla_x(u \cdot \nabla_x Y) = 0 \\ (\rho e)_t + \operatorname{div}_x(\rho e u - \sigma^T u) = 0 \end{cases} \tag{1}$$

where $Y(x,t)$ are the backward characteristics of the problem, $u(x,t)$ the velocity, $e(x,t)$ the total energy per unit mass, $\rho(x,t)$ the density and $\sigma(x,t)$ the Cauchy stress tensor. To close the system a constitutive law is chosen. The internal energy per unit mass is given by

$$\varepsilon = e - \frac{1}{2}|u|^2 = \frac{\kappa(s)}{\gamma - 1}\left(\frac{1}{\rho} - b\right)^{1-\gamma} - a\rho + \frac{p_\infty}{\rho} + \frac{\chi}{\rho_0}(\operatorname{Tr}(\overline{B}) - 3) \tag{2}$$

where $\kappa(s) = \exp(s/c_v)$, $s(x,t)$ is the entropy and $\overline{B}(x,t)$ is the modified left Cauchy-Green tensor given in 3D by

$$\overline{B}(x,t) = [\nabla_x Y(x,t)]^{-1}[\nabla_x Y(x,t)]^{-T}/J(x,t)^{2/3} \qquad J(x,t) = \det([\nabla_x Y(x,t)])^{-1} \tag{3}$$

The constants $\gamma, a, b, p_\infty, \rho_0$, have the usual meaning and χ is the shear modulus. The two first terms of (2) represent a Van der Waals gas, the third one a stiffened gas and the last one represent a Neo-Hookean elastic solid. The stress tensor σ is then derived from this constitutive law

$$\sigma = -p(\rho, s)I + 2\chi J^{-1}\left(\overline{B} - \frac{\text{Tr}(\overline{B})}{3}I\right) \tag{4}$$

where the pressure p is given by

$$p(\rho, s) = -p_\infty - a\rho^2 + \kappa(s)\left(\frac{1}{\rho} - b\right)^{-\gamma} \tag{5}$$

3 Numerical scheme

Let $x = (x_1, x_2, x_3)$ be the coordinates in the canonical basis of $\mathbb{R}^3$, $u = (u_1, u_2, u_3)$ the velocity components, $Y = (Y^1, Y^2, Y^3)$ the components of Y and σ^{ij} the components of the stress tensor σ. Also, let us denote by $,k$ the differentiation with respect to x_k. Our scheme is based on a directional splitting on a cartesian mesh. When computing the numerical fluxes at cell interfaces in the x_1 direction we have $(Y^i_{,2})_t = (Y^i_{,3})_t = 0$ thus $Y^i_{,2}$ and $Y^i_{,3}$ are constants. The governing equations in conservative form in the x_1 direction become

$$\Psi_t + (F(\Psi))_{,1} = 0 \tag{6}$$

with $\phi_i = \rho u_i$ and $\psi = \rho e$

$$\Psi = \begin{pmatrix} \rho \\ \phi_1 \\ \phi_2 \\ \phi_3 \\ Y^1_{,1} \\ Y^2_{,1} \\ Y^3_{,1} \\ \psi \end{pmatrix} \qquad F(\Psi) = \begin{pmatrix} \phi_1 \\ \frac{(\phi_1)^2}{\rho} - \sigma^{11} \\ \frac{\phi_1\phi_2}{\rho} - \sigma^{21} \\ \frac{\phi_1\phi_3}{\rho} - \sigma^{31} \\ \frac{\phi_1 Y^1_{,1} + \phi_2 Y^1_{,2} + \phi_3 Y^1_{,3}}{\rho} \\ \frac{\phi_1 Y^2_{,1} + \phi_2 Y^2_{,2} + \phi_3 Y^2_{,3}}{\rho} \\ \frac{\phi_1 Y^3_{,1} + \phi_2 Y^3_{,2} + \phi_3 Y^3_{,3}}{\rho} \\ \frac{\phi_1\psi - (\sigma^{11}\phi_1 + \sigma^{21}\phi_2 + \sigma^{31}\phi_3)}{\rho} \end{pmatrix}$$

The numerical fluxes are computed with a HLLC approximate Riemann solver. This solver requires the analytical expression of the wave velocities which are the eigenvalues of the Jacobian of $F(\Psi)$. The wave velocities are defined locally by infinitesimal variations of the conservative variables. Therefore the energy equation can be replaced by the transport equation on the entropy $s_t + u \cdot \nabla s = 0$ and the wave velocity calculations are performed at fixed entropy. We introduce the notation

$$\Sigma = [\nabla\sigma][\nabla Y] := \begin{pmatrix} \sigma^{11}_{,1} & \sigma^{11}_{,2} & \sigma^{11}_{,3} \\ \sigma^{21}_{,1} & \sigma^{21}_{,2} & \sigma^{21}_{,3} \\ \sigma^{31}_{,1} & \sigma^{31}_{,2} & \sigma^{31}_{,3} \end{pmatrix} \begin{pmatrix} Y^1_{,1} & Y^1_{,2} & Y^1_{,3} \\ Y^2_{,1} & Y^2_{,2} & Y^2_{,3} \\ Y^3_{,1} & Y^3_{,2} & Y^3_{,3} \end{pmatrix} \tag{7}$$

where $\sigma^{ij}_{,k}$ denote the derivative of σ^{ij} with respect to $Y^k_{,1}$. The wave speeds are then given by

$$\Lambda_E = \left\{ u_1, u_1 \pm \sqrt{\frac{\alpha_1}{\rho}}, u_1 \pm \sqrt{\frac{\alpha_2}{\rho}}, u_1 \pm \sqrt{\frac{\alpha_3}{\rho}} \right\}$$

where α_1, α_2 and α_3 are the roots of the polynomial of third order

2

$$X^3 + \text{Tr}(\Sigma)X^2 + \text{Tr}(\text{Cof}((\Sigma))X + \text{Det}(\Sigma) = 0 \tag{8}$$

Therefore, the conditions for the system (6) to be hyperbolic are $\alpha_1 > 0$, $\alpha_2 > 0$ and $\alpha_3 > 0$.

The numerical flux function $\mathcal{F}(\Psi_l, \Psi_r)$ is computed using the HLLC [5] approximate solver modified according to [4] at the multimaterial interface. The wave pattern involves seven waves in the exact problem, but the HLLC approximate solver approaches the solution using three waves and thus defining two intermediate states Ψ^- and Ψ^+ (see Fig 1). The three waves are the contact discontinuity and the two fastest waves. Rankine Hugoniot conditions are used to determine the two intermediate states.
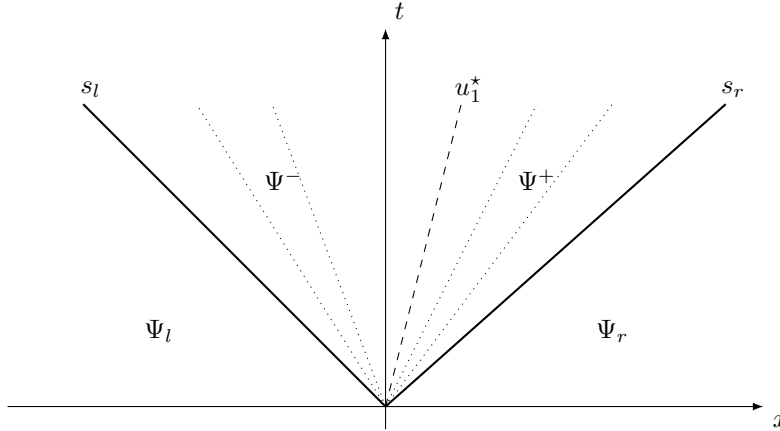

Figure 1: HLLC solver wave pattern.

The multimaterial solver is detailed in 1D for sake of clarity. In 3D we use exactly the same method in the three directions. We consider a case where the material discontinuity is between the cell centers $k-1$ and k. The material discontinuity can separate materials with different constitutive laws or discontinuous initial states of the same material. The main idea of the multimaterial solver is that we take (see Fig 2)

$$\mathcal{F}^l_{k-1/2} = \mathcal{F}^- \qquad \mathcal{F}^r_{k-1/2} = \mathcal{F}^+ \tag{9}$$

where $\mathcal{F}^- = F(\Psi^-)$ and $\mathcal{F}^+ = F(\Psi^+)$. As for ghost-fluid methods, the scheme is locally non conservative since $\mathcal{F}^- \neq \mathcal{F}^+$, but it is consistent since $\mathcal{F}^{\pm}$ are regular enough functions of the states to the left and to the right of the interface and $\mathcal{F}^+ = \mathcal{F}^-$ when those states are identical. As shown in [4] the error in conservation is negligible: the shock speeds and positions are correctly predicted and the results are oscillation free. Coherently with the fully Eulerian approach, a level set function is used to follow the interface separating the two materials. The scheme is extended to second order accuracy in space with a piecewise-linear slope reconstruction (MUSCL).
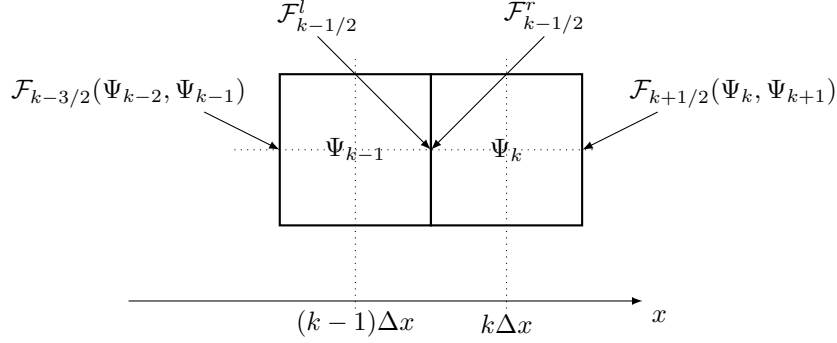
Figure 2: Fluxes at the material discontinuity

4   3D numerical results

We show in this section 3D generalisations of the shock bubble interaction tests and of the impact of a projectile in air. The computations are performed with a parallel code and last for 24h on 64 processors for impacts and 14h on 96 processors for Shock-bubble interactions.

TC	Media	ρ [kg/m^3]	u_1 [m/s]	p [Pa]	γ	a	b	p_∞ [Pa]	χ [Pa]
1	Air (pre-shock)	1.225	0	101325	1.4	0	0	0	0
	Air (post-shock)	1.6861	-113.534	159059					
	Helium	0.2228	0	101325	1.648	0	0	0	0
2	Water (pre-shock)	1000	0	10^5	4.4	0	0	$6 \cdot 10^8$	0
	Water (post-shock)	1230	-432.69	10^9					
	Air	1.2	0	10^5	1.4	5	10^{-3}	0	0
3	Copper (plate)	8900	0	10^5	4.22	0	0	$3.42 \cdot 10^{10}$	$5 \cdot 10^{10}$
	Copper (projectile)	8900	800	10^5					
	Air	1	0	10^5	1.4	0	0	0	0
4	"Fluid limit" (plate)	8900	0	10^5	4.22	0	0	$3.42 \cdot 10^{10}$	0
	"Fluid limit" (projectile)	8900	800	10^5					
	Air	1	0	10^5	1.4	0	0	0	0

Table 1: Three-dimensional test case description.

4.1   Shock-Bubble interaction

We consider two shock-bubble interaction test cases involving two different fluids. The boundary conditions are reflection on upper and lower borders and homogeneous Neumann conditions for inlet and outlet.

Air-Helium Shock-Bubble interaction

The test case 1 is the propagation of a Mach 1.22 shock moving in air, through an helium bubble. The initial configuration and the physical parameters are described on Fig. 3 and in Table 1. The computation is performed on a $500 \times 200 \times 200$ points grid. The zero iso-value of the level set function is presented at different times on Fig. 4.
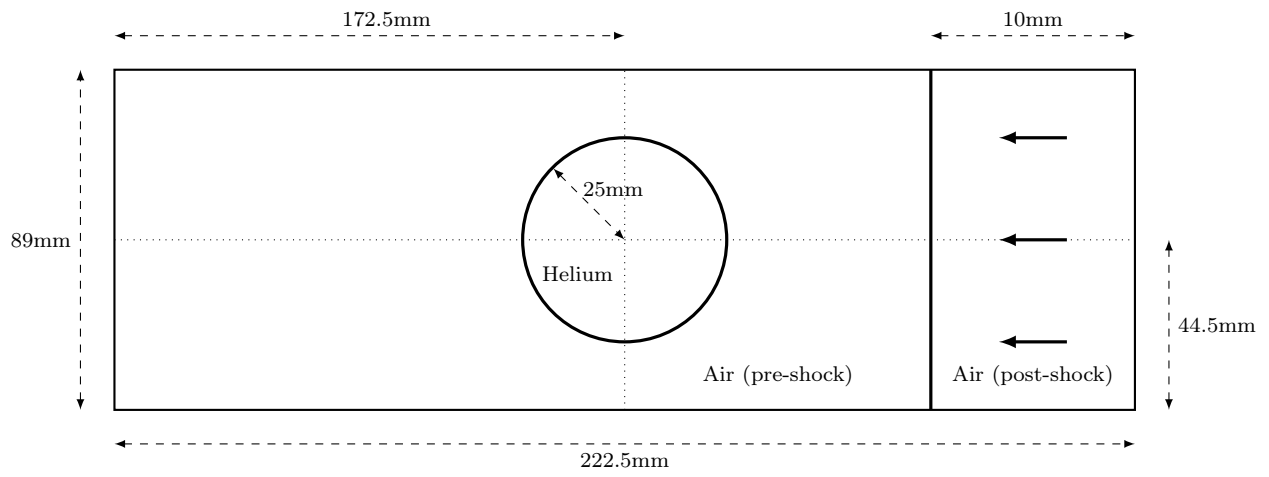
4

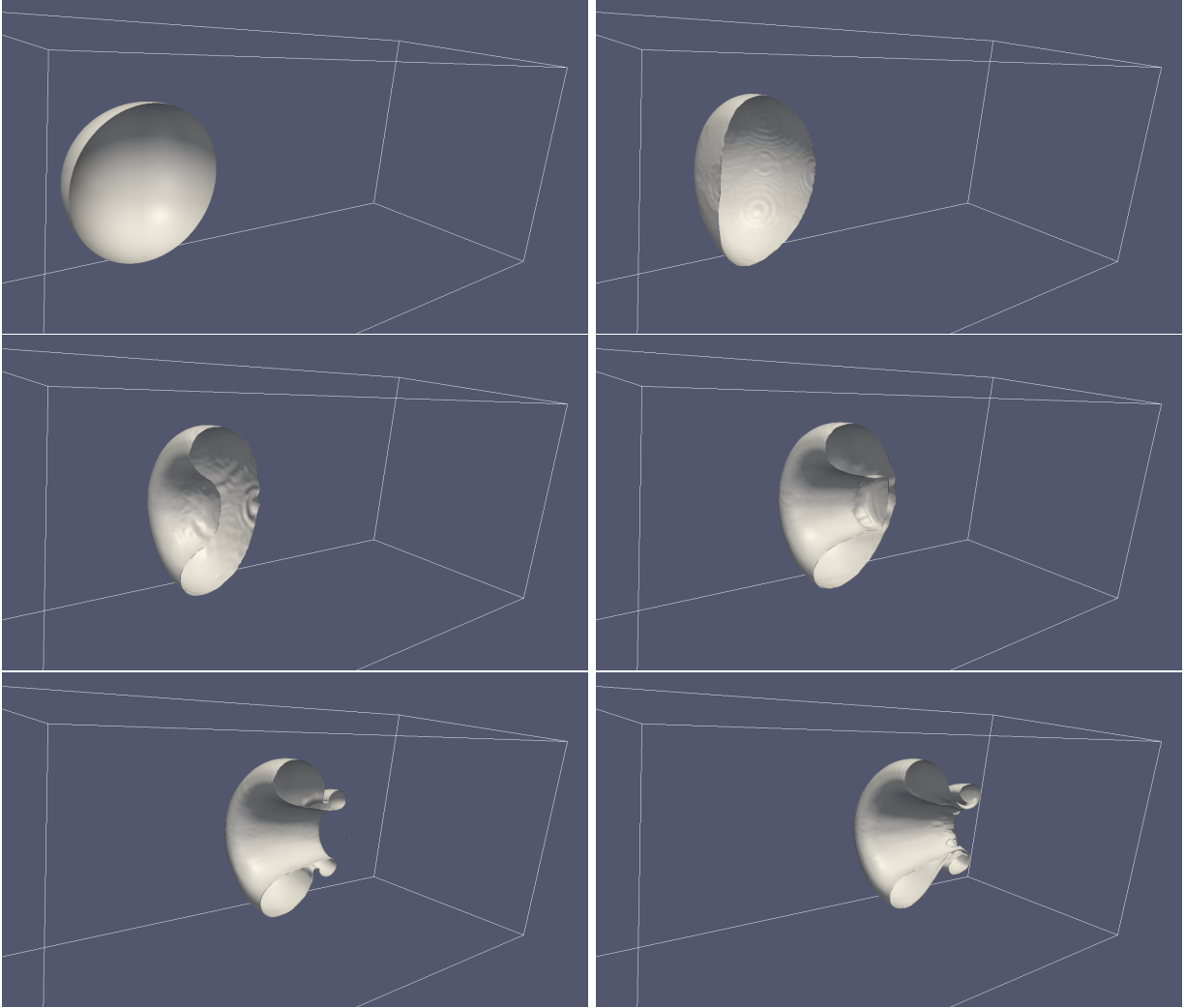Figure 3: Sketch of a middle section of the 3D initial configuration for TC1

Figure 4: Interaction of a Mach 1.22 shock in air and an helium bubble (TC1). Pictures at $t = 0\mu s, 105\mu s, 211\mu s, 317\mu s, 446\mu s, 575\mu s$. From left to right, top to bottom.

Air-water Shock-Bubble interaction

The test case 2 involves a Van der Waals bubble and a Mach 1.422 shock in a stiffened gas. The computational domain is $[-0.2, 1] \times [0, 1] \times [0, 1]$, the initial configuration and the physical parameters are described in Fig. 5 and in Table 1 . This test case is more severe compared to the previous one since it presents larger density ratios. The computational grid is $480 \times 400 \times 400$. The results are presented in Fig. 6.
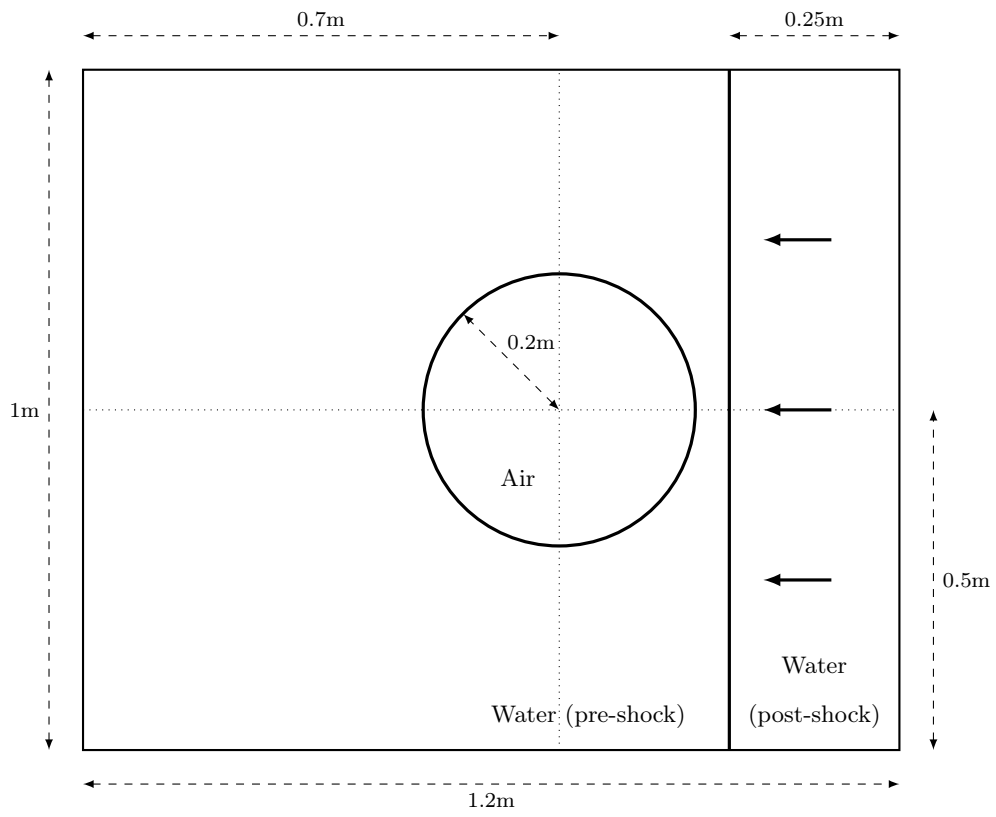
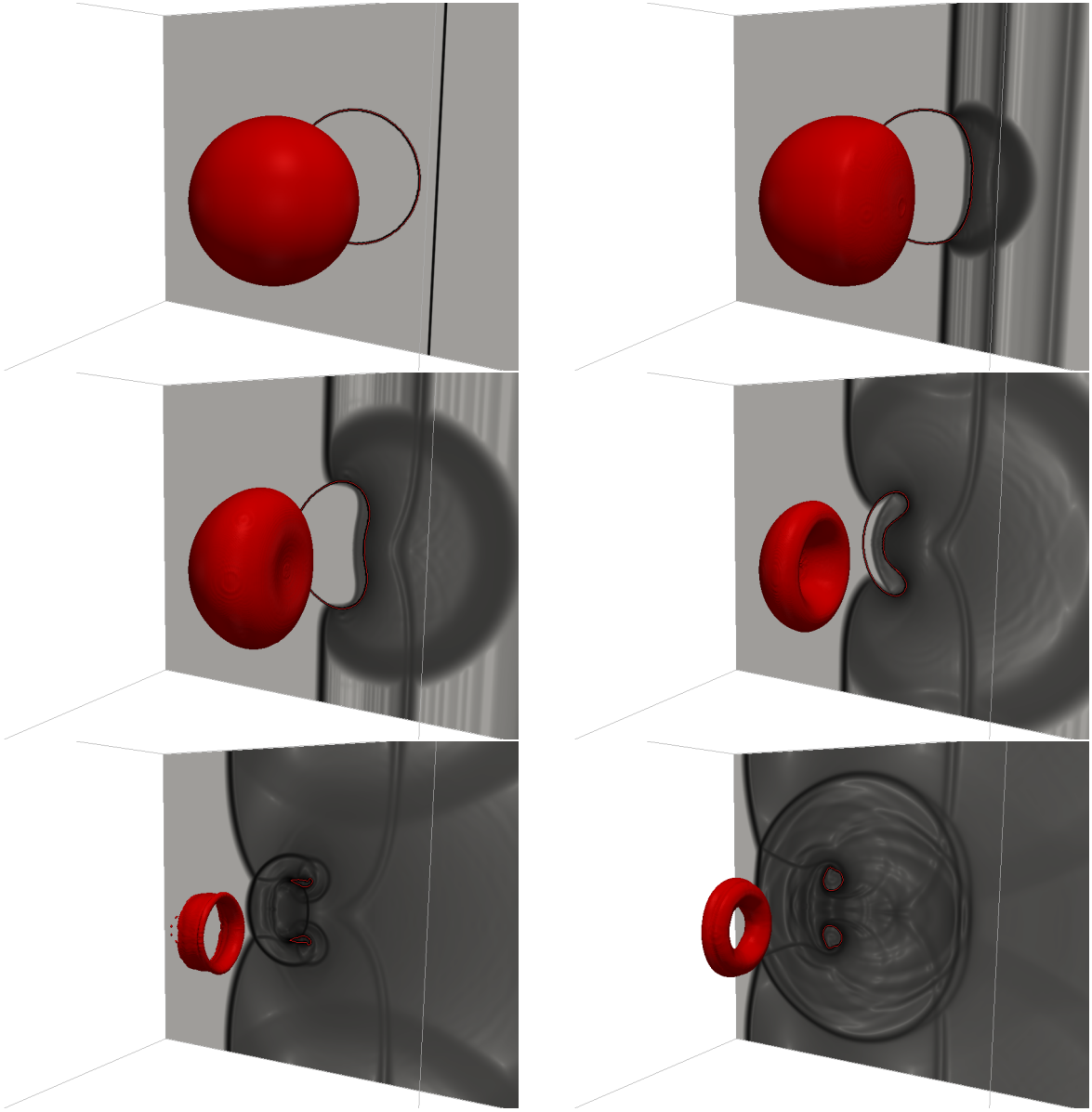Figure 5: Sketch of a middle section of the 3D initial configuration for TC2

Figure 6: Interaction of a Mach 1.422 water shock and an air bubble (TC2). Interface and schlieren of the slice $z = 0.5$ at time $t = 0\mu s, 37\mu s, 73\mu s, 110\mu s, 147\mu s, 195\mu s$. From left to right, top to bottom.

The bubble is strongly compressed, it breaks and swirls.

4.2 Impacts

Finally, we present two impact simulations of a 800 m/s projectile on a plate in air (TC3 and TC4). The computational domain is $[-0.5, 0.5]^3$, the initial configuration and the physical parameters are described in Fig. 7 and in Table 1 . The projectile and the plate are adjacent at initial time. Homogeneous Neumann conditions are imposed at the borders. Two computations are performed on a 200^3 mesh, changing the shear parameter ($\chi = 5 \cdot 10^{10}$ in TC3 and $\chi = 0$ in TC4, see Table 1).
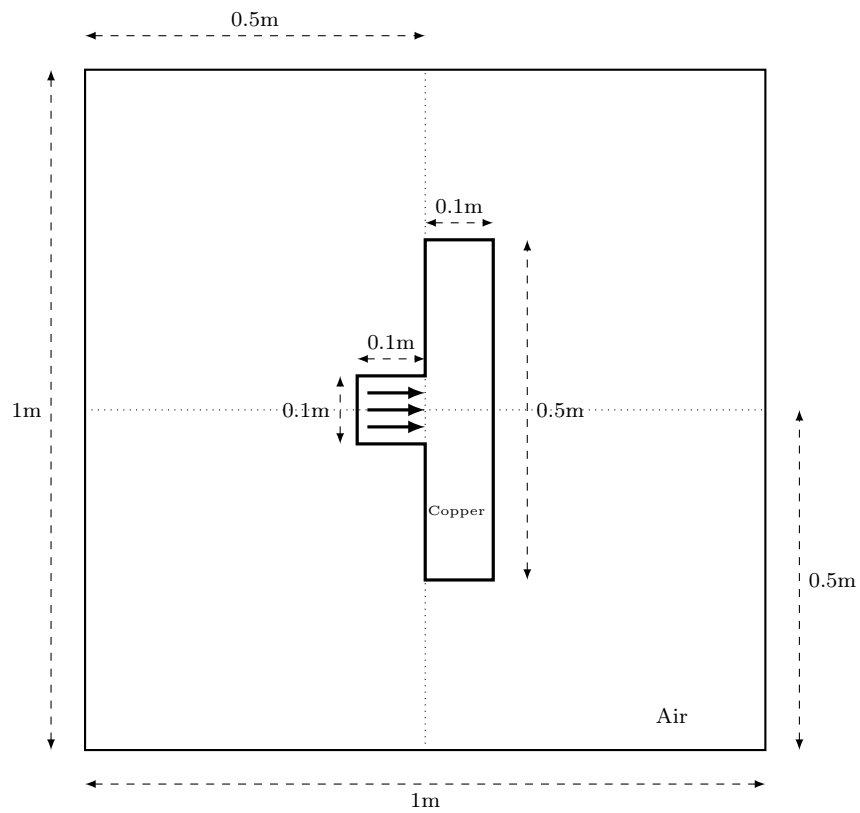
Figure 7: Sketch of a middle section the 3D initial configuration for the impact test cases TC3 and TC4

The elastic material is deformed and oscillates while being displaced rightward (leftward in Fig 8 and Fig 9 as the pictures have been rotated 180 degrees)
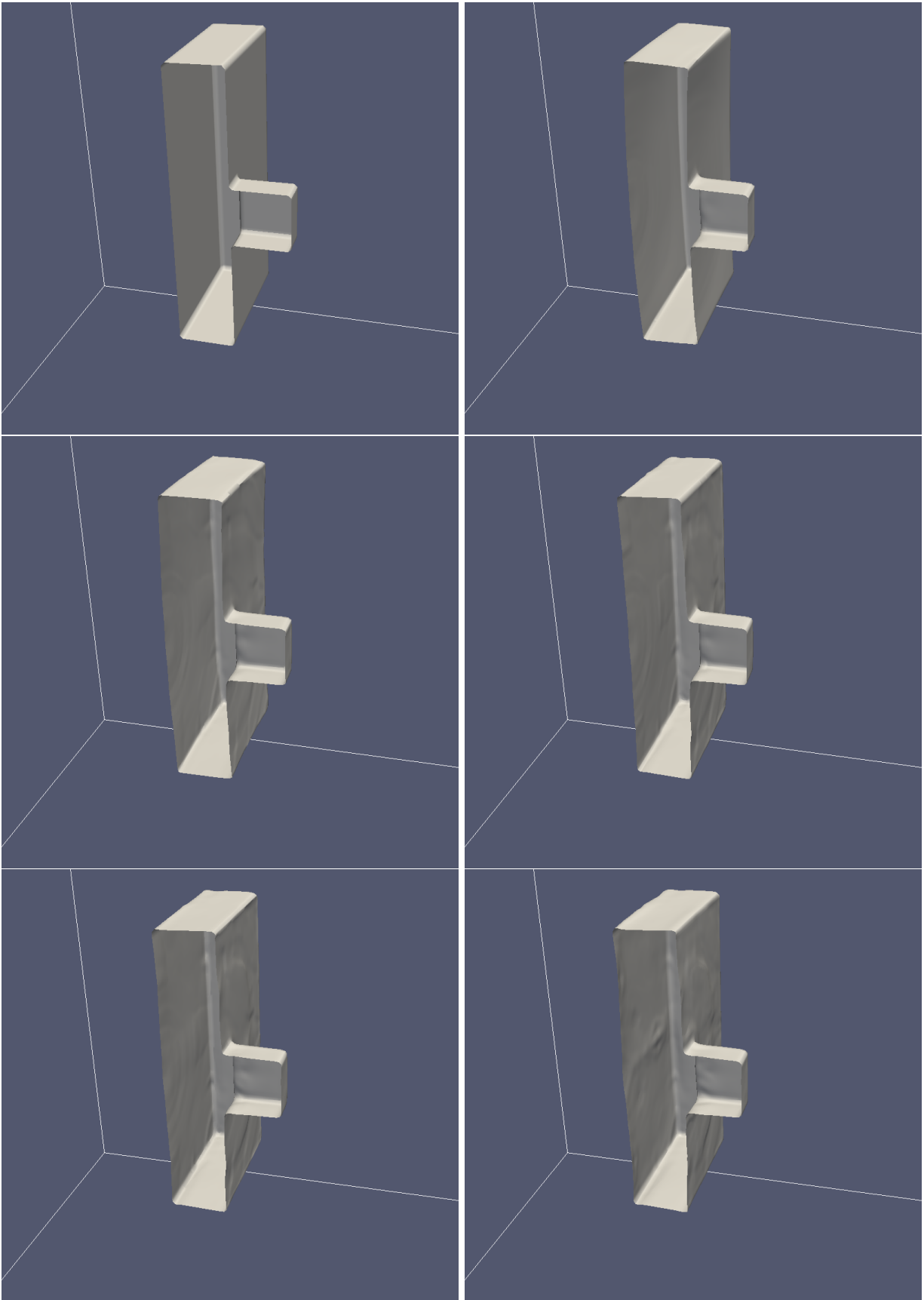
Figure 8: Impact of a projectile on a plate for $\chi = 5 \cdot 10^{10}$Pa (TC3). Interface at $t = 0\mu s, 118\mu s, 237\mu s, 355\mu s, 473\mu s, 592\mu s$. From left to right, top to bottom.

In Fig. 9, one can see the results for $\chi = 0$ (TC4) which corresponds to the fluid limit. The plate undergoes extreme deformations as there is no force to bring back the structure to its reference configuration.
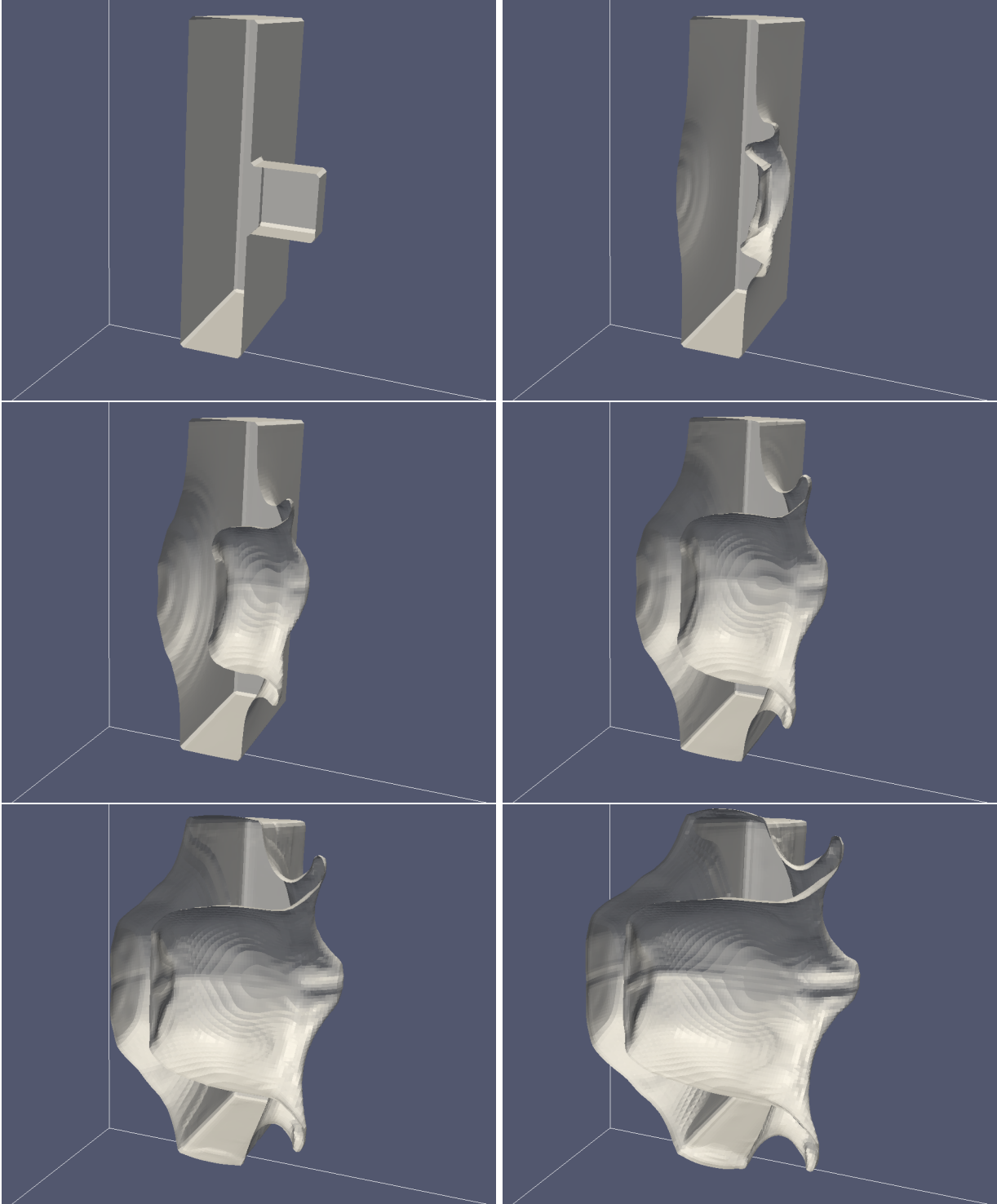

Figure 9: Impact of a projectile on a plate for $\chi = 0$ (TC4). Interface at $t = 0\mu s, 118\mu s, 237\mu s, 355\mu s, 473\mu s, 592\mu s$. From left to right, top to bottom.

5 Conclusion and Future Work

This numerical approach is constrained with the time scale of the elastic waves. This is a very strong limit for rigid materials. Except for specific problems such as impacts or in general fast-dynamical processes, the relevant physical phenomena take place on the time scale determined by the fluid velocity. These significantly different time scales introduce stability, accuracy and efficiency problems that are well known in compressible fluids. Future work will include exploration of these issues for compressible multimaterial flows.

References

[1] S.K Godunov. *Elements of continuum mechanics*. Nauka Moskow. 1978.

[2] A. Iollo, T. Milcent, H. Telib. A sharp contact discontinuity scheme for multimaterial models. *Finite Volumes for Complex Applications VI*. Springer Proceedings in Mathematics 4, 2011.

[3] Y. Gorsse, A. Iollo, T. Milcent, H. Telib. Accurate sharp interface scheme for multimaterial. *International Conference on Computational Fluid Dynamics (ICCFD7)*. Hawaii, 2012.

[4] Y. Gorsse, A. Iollo, T. Milcent, H. Telib. A simple Cartesian scheme for compressible multimaterial. *Journal of Computational Physics*. Vol 272, p772-798, 2014.

[5] E.F Toro, M. Spruce, W. Speares. Restoration of the contact surface in the HLL-Riemann solver. *Shock Waves*. Vol 4, p25-34, 1994.